Journal of Engineering Mathematics **37:** 375–395, 2000.

The evaluation of the Biot–Savart integral

J.-C. SUH
Department of Naval Architecture and Ocean Engineering, Seoul National University, RIMSE, Seoul, 151–742, Korea

(Received: 16 October 1997; accepted in revised form 10 May 1999)

Abstract. A computational method is described for evaluating the Biot–Savart integral. The approach emphasizes the transformation of the involved integrand into suitable forms, from which integral theorems can be used to reduce the volume integral into line integrals. This method is applied to the case where the density of vorticity (current) distributed over a volumetric element bounded by planar surfaces (straight lines in two-dimensional) is constant and/or linear. The resulting expressions for the volume integral involve closed-form expressions for line integrals along the edges of the element. The evaluation of the line integrals is treated independently for each of the edges as opposed to direct numerical integration. The closed-form formulas are expressed in terms of geometric parameters of the element edges. The versatility of the proposed scheme is demonstrated by applying it to two examples: (i) two-dimensional lid-driven cavity flows; (ii) a magnetic field induced by a toroidal tokamak coil. A systematic extension to the general cases where the vorticity distribution is of higher-order polynomial form is also presented.

Key words: Biot–Savart law, linearly varying density, transformation of integrands, contour integrals, closed-form expressions.

1. Introduction

Vector mathematical identities involving an integral of singularities distributed over a surface and a field can be employed to define fields values of a vector variable of interest at a point within a field. For example, the field values of an irrotational and solenoidal vector can be obtained from the integrals over the sole surfaces bounding the field. In boundary-integral methods which were inspired by the work of Hess and Smith [1, 2] for potential flow problems of an incompressible fluid, the surface integrals involved may be evaluated on the boundary if it is assumed that the bounding surfaces are composed of a set of discrete panels and a certain variation in the boundary values of the dependent variable in space (over the panels) and time. For other problems related to rotational and solenoidal vector fields, a volume integral exists, the so-called Biot–Savart integral. It is well known that the Biot–Savart integral represents a formula in electromagnetic field theory that relates a field distribution of electric current to the induced magnetic field (see *e.g.*, [3]). In a manner analogous with the magnetic field induced by the given distribution of current, this induction law has been also applied to hydro- and aerodynamics by many workers: a distribution of vorticity in a field induces the velocity field whose curl becomes the given value of vorticity everywhere [4, Chapter 2], [5, Chapter 2]. In vortex methods for viscous flow analyses–especially in the vorticity-velocity integro-differential formulations (see *e.g.*, [6]) the Biot–Savart integral must be evaluated at appropriate field points within the discretized fluid domain. With N elements used in discretizing the fluid domain over which vorticity is distributed, $O(N^2)$ evaluations of the Biot–Savart integral may be required in order to calculate the velocity field. The evaluation

of the Biot–Savart integral is, therefore, an important task in the numerical implementations associated with computational electromagnetics and fluid mechanics.

For a distributed vorticity (current) field $\boldsymbol{\omega}$ in a fluid (current-carrying) region V, the general form of the Biot–Savart law is

$$\mathbf{q} = \int_V \boldsymbol{\omega} \times \nabla G \, \mathrm{d}V, \tag{1}$$

where $\mathbf{q}$ is the induced velocity (magnetic) field and G the fundamental function, defined by

$$G = \begin{cases} \dfrac{1}{4\pi r} & \text{in 3-dimensions,} \\ -\dfrac{1}{2\pi} \log r & \text{in 2-dimensions.} \end{cases}$$

Hereafter, ∇ denotes the gradient, divergence, and curl differential operator with respect to integration variables $\boldsymbol{\xi}$, and r the distance between a field point $\mathbf{x}$ and an integration point $\boldsymbol{\xi}$.

Several computational methods for evaluating the Biot–Savart integral have been developed and used in the context of computational electromagnetism and fluid dynamics. Since it is impossible to evaluate the volume integral analytically for general geometric forms of integration regions, the regions may be subdivided into elements of simpler forms for which it can be performed. The accuracy of the field computation depends on the exact representation of the form of the vorticity distribution regions as well as the density distribution. The simplest model in this respect is to approximate the actual volume distribution by concentrated discrete filaments. The volume integral then reduces to a one-dimensional integration along the straight or curved filaments [7, 8]. However, this model is not appropriate for the cases in which the velocity (magnetic) field distribution within the vorticity (current-carrying) field is needed. In this case, the field value becomes infinite when the field point approaches the filament.

Using current sheets for better approximation, Urankar [9] presented analytical expressions for the magnetic field of a thin circular conic cylinder segment carrying a constant peripheral electric current. The expressions consist of Jacobian elliptic functions and elliptic integrals of the first, second, and third kind. Therefore a numerical evaluation of another type of integral will be needed. In the context of fluid dynamics, the results for two-dimensional Biot–Savart integrations are given in [10–12]. Following Hess and Smith's procedure [2] which was well established in potential flow analyses using boundary-integral methods, Cielak and Kinney [10] obtained an analytical expression for the velocity induced by a vorticity distribution of constant density over a rectangular element in two-dimensions. The concept stressed in their work is that a surface integral over the element can be expressed as a superposition of integrals over a set of triangular regions with a common apex at a given field point and bases conforming to the four sides of the rectangular element. The procedure is accurate in the algorithmic sense. Their derivation is, however, restricted to constant-density distributions over rectangular elements. In subsequent extensions [11–14], linear distributions have been used on triangular elements to provide a continuous description of the distribution. The corresponding integral for these distributions can be performed on the basis of algebraic manipulations in a manner similar to Hess and Smith's procedure.

A complete three-dimensional volume integral of Equation (1) is used in [15, 16] for evaluating the three-dimensional magnetic field of a circular arc segment of a constant current-carrying conductor of rectangular cross section in terms of elliptic functions and elliptic

integrals. Since such a curved conductor may, in general, be approximated by a chain of wedge-shaped segments, its magnetic field is given by a sum over the partial contributions of each segment [17]. For a given volume distribution of electric current over a segment, the magnetic field can be determined by modeling the current distribution in terms of a distribution of fictitious magnetization inside the segment volume, surface currents and magnetic charges. This concept is the same as that of vector integral identities, which has been used in the boundary element methods for solving incompressible viscous flow problems [18]. The corresponding results for a straight segment of the same rectangular cross section with trapezoidal sides are given in [19, 20].

The goal of this paper is to develop a more elegant derivation and to extend these earlier analyses. Efficient numerical analysis schemes for a linear distribution of vorticity (current) over a surface in two-dimensions or over a volume in three-dimensions are presented on the basis of transformations of the integrals. It will be shown that the induced velocity (magnetic) field due to a vorticity (current) distribution with linear strength can be derived from a sum of line integrals along the edges of a subdivided element. The derivation used here employs Stokes's and/or Gauss's theorem, by which the velocity (magnetic) field can be expressed in terms which are dependent only on the properties of each edge: namely, the terms of the position of a field point relative to each edge. In this manner, an analysis associated with direct calculation of the triple (double in two-dimensional) integral over the element can be avoided. An additional feature of the present derivation is that it is valid for an arbitrary element bounded by planar surfaces (straight lines in two-dimensional). The versatility of the proposed scheme is demonstrated by applying it to two examples. We consider a vorticity-based integro-differential formulation for the numerical solution of a two dimensional cavity flow driven by shear and body forces. A computation of the magnetic induction on a perimeter inside the field coil of rectangular cross section for a typical tokamak magnet is performed in order to illustrate the validation of the present derivation. A systematic extension to the general cases where the vorticity distribution is of higher-order polynomial form is also presented. Since an analogy between vorticity and electric current exists, as well as between velocity and magnetic field, we shall use only the words 'vorticity' and 'velocity' in the following sections unless otherwise stated.

2. Biot–Savart integral in two-dimensional

A quadrilateral element is, without loss of generality, taken for the present analysis. The complete induced field is constructed by superposing the field contributions due to the individual elements. For any polygon, we can easily deduce the corresponding results from the expression, Equation (4) below, by taking into account the number of sides of the polygon in the summation of the contributions for each side. The vertices with coordinates (ξ_i, η_i) are denoted by $\boldsymbol{\xi}_i$, as shown in Figure 1, where each vertex is indicated by the index i. The induced velocity ($\mathbf{q}$) at any arbitrary field point $P(\mathbf{x})$ with coordinates (x, y) due to a distribution of vorticity over the domain of the element S is

$$\mathbf{q} = -\frac{\mathbf{k}}{2\pi} \times \int_S \omega \nabla(\log r)\, \mathrm{d}S, \tag{2}$$

where $r = |\mathbf{r}| = |\boldsymbol{\xi} - \mathbf{x}|$ and ω is the scalar plane component of the vorticity vector, $\boldsymbol{\omega}(\equiv \omega\mathbf{k})$.

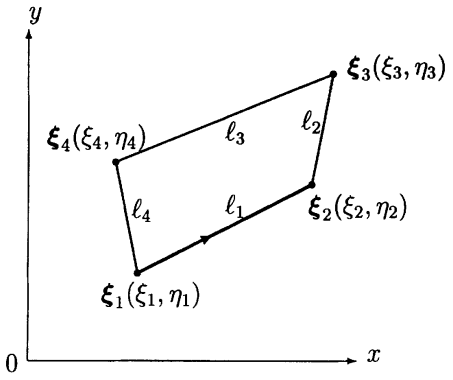

Figure 1. Definition of a quadrilateral element.

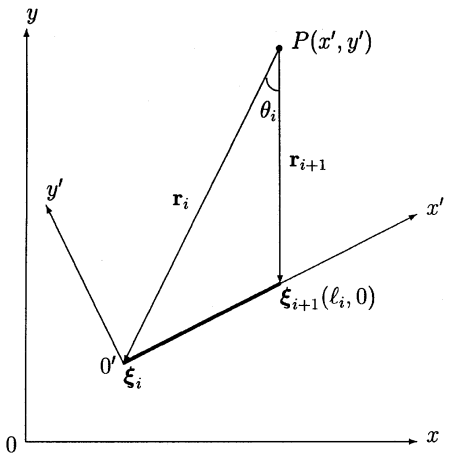

Figure 2. Definition sketch of the local coordinate system (x', y').

The integrand can be transformed into, through simple vector operations,

$$\omega \nabla(\log r) = \nabla(\omega \log r) - \tfrac{1}{2}\{\nabla \cdot (\mathbf{r} \log r) - 1\}\nabla\omega. \tag{3}$$

For a vorticity distribution of linear-variation density, we can convert the surface integral in Equation (2) into line integral terms, by applying the Gauss theorem with the transformed integrand given in Equation (3)

$$\int_S \omega \nabla(\log r)\, \mathrm{d}S = \tfrac{1}{2} \oint_C \mathbf{n}\omega(\log r^2 + 1)\, \mathrm{d}C - \tfrac{1}{2}\nabla\omega \oint_C (\mathbf{n} \cdot \mathbf{r}) \log r\, \mathrm{d}C.$$

Here the contour integrals are performed along the perimeter (C) of the element in a counterclockwise direction, and $\mathbf{n}$ is the unit normal vector on the boundary of the element in the sense of a right-handed rule, *i.e.*, $\mathbf{n} = \mathbf{s} \times \mathbf{k}$ where $\mathbf{s}$ is the unit directional vector of the contour integral path. Then $\mathbf{k}$, $\mathbf{n}$ and $\mathbf{s}$ constitute a right-handed triple of orthogonal unit vectors.

The resulting expressions for the velocity field include the line integrals only along the boundary contour of the element. Let the value of the line integral along each straight edge of the element be $\mathbf{I}_i$. It then follows that

$$\mathbf{q} = -\frac{\mathbf{k}}{2\pi} \times \left(\sum_{i=1}^{4} \mathbf{I}_i \right), \tag{4}$$

where, with the side of length ℓ_i,

$$\mathbf{I}_i = \tfrac{1}{2}\mathbf{n}_i \int_0^{\ell_i} \omega(\log r^2 + 1)\, \mathrm{d}C - \tfrac{1}{4}\nabla\omega(\mathbf{n}_i \cdot \mathbf{r}) \int_0^{\ell_i} \log r^2\, \mathrm{d}C.$$

It is seen that the line integral for each side can be treated independently. It is sufficient, therefore, to consider only one side of the polygon for the purpose of integration. The essential task is to evaluate the line integrals along a straight segment from $\boldsymbol{\xi}_i$ to $\boldsymbol{\xi}_{i+1}$ with linear variation of ω over it.

For the evaluation of the associated integrals, we take a local coordinate system (x', y') in the plane through the field point $\mathbf{x}$ and the side concerned, such that the side lies on the x'-axis

and one end point of the side is at the origin of the coordinates (See Figure 2). The integration is performed along the positive x'-axis. The reason for choosing the local coordinate system as such is because the integration is more compact and systematic than that for the case of the global coordinate system, even though both procedures, in fact, produce identical results. Of course the coordinates of the field point in the global coordinate system must be transformed into the local coordinate systems of the respective sides, and the computed field components must then be defined in the global coordinate system to superpose the contributions due to the respective sides.

The local coordinates are related to the vectors defined in the global coordinate system as: $x' = -\mathbf{r}_i \cdot \mathbf{s}_i$ and $y' = (\mathbf{r}_i \times \mathbf{s}_i) \cdot \mathbf{k}$. This transformation implies the projections of distance vectors between the field point P and the end points of the segment on the x'- and y'-axis. Let us denote the distances between the two end points of the side and the field point by $r_i = \sqrt{x'^2 + y'^2}$ and $r_{i+1} = \sqrt{(\ell_i - x')^2 + y'^2}$, respectively. After a substantial amount of algebraic manipulations (see [21, pp. 81–84] for integral formulae), the following result for $\mathbf{I}_i$ can be obtained

$$\mathbf{I}_i = \tfrac{1}{2}\mathbf{n}_i\{\omega_i(\ell_i + I^{(1)}) + (\nabla\omega \cdot \mathbf{s}_i)(\tfrac{1}{2}\ell_i^2 + I^{(2)})\} - \tfrac{1}{4}\nabla\omega(\mathbf{n}_i \cdot \mathbf{r})I^{(1)},$$

where ω_i denotes the vorticity value at the ith vertex,

$$I^{(1)} = (\ell_i - x')\log r_{i+1}^2 + x' \log r_i^2 - 2\ell_i + 2|y'|\theta_i, \tag{5}$$

$$I^{(2)} = \tfrac{1}{2}(r_{i+1}^2 \log r_{i+1}^2 - r_i^2 \log r_i^2) - \tfrac{1}{2}\ell_i^2 + \ell_i x' + x' I^{(1)}, \tag{6}$$

and

$$\theta_i = \tan^{-1} \frac{|y'|\ell_i}{r_i^2 - \ell_i x'}.$$

Here the pair of arctangents appearing in this evaluation have been combined by using the trigonometric formulae. Eventually it is seen that θ_i denotes the included angle between distance vectors of the segment end points as viewed from the field point P (see Figure 2). Thus, the included angle is uniquely measured as a value between 0 and π without considering the separate arguments of the arctangent function, since the numerator of the argument of the arctangent is non-negative. Note that the terms $I^{(1)}$ and $I^{(2)}$ given by Equations (5) and (6) are determinate when the field point is on the extensions of the side. For example, if the field point approaches one of the end points of the side, we have finite values according to L'Hospital's rule (for the indeterminate form $0 \cdot \infty$).

3. Biot–Savart integral in three-dimensional

The induced velocity due to a vorticity distribution over an element whose boundary is composed of planar panels, can be expressed in a volume form analogous to Equation (2):

$$\begin{aligned}\mathbf{q} &= \frac{1}{4\pi}\int_V \boldsymbol{\omega} \times \nabla\left(\frac{1}{r}\right) \mathrm{d}V \\ &= \frac{1}{4\pi}\int_V \left\{\frac{1}{r}(\nabla \times \boldsymbol{\omega}) - \nabla \times \left(\frac{1}{r}\boldsymbol{\omega}\right)\right\} \mathrm{d}V.\end{aligned} \tag{7}$$

The vorticity distribution is assumed to be linear so that $(\nabla \times \boldsymbol{\omega})$ is constant. By using the divergence (Gauss) theorem, Equation (7) can be reduced to

$$4\pi \mathbf{q} = (\nabla \times \boldsymbol{\omega}) \int_V \frac{1}{r}\,\mathrm{d}V - \oint_S \mathbf{n} \times \left(\frac{1}{r}\boldsymbol{\omega}\right)\,\mathrm{d}S, \tag{8}$$

where S is the surfaces bounding the volume V and $\mathbf{n}$ is the outward normal unit vector on the bounding surfaces.

In order to evaluate the volume integral term in Equation (8), we use here Green's second identity for a scalar function ϕ such that $\nabla^2\phi = 1$

$$\int_V \frac{1}{r}\,\mathrm{d}V = -\alpha\phi(\mathbf{x}) - \oint_S \left\{\phi\mathbf{n}\cdot\nabla\frac{1}{r} - \frac{\mathbf{n}\cdot\nabla\phi}{r}\right\}\,\mathrm{d}S, \tag{9}$$

where α is constant. When $\mathbf{x}$ is inside the volumetric region V, α is 4π. If $\mathbf{x}$ is on the boundary of V, it is 2π. For $\mathbf{x}$ outside the volume, this value is zero. Equation (8) can then be expressed as a sum of integrals over the bounding planar surfaces as

$$\begin{aligned} 4\pi\mathbf{q} \;=\; & -(\nabla\times\boldsymbol{\omega})\left[\alpha\phi(\mathbf{x}) + \oint_S \left\{\phi\mathbf{n}\cdot\nabla\left(\frac{1}{r}\right) - \frac{\mathbf{n}\cdot\nabla\phi}{r}\right\}\,\mathrm{d}S\right] \\ & - \oint_S \mathbf{n}\times\left(\frac{1}{r}\boldsymbol{\omega}\right)\,\mathrm{d}S, \\ =\; & -(\nabla\times\boldsymbol{\omega})\alpha\phi(\mathbf{x}) - \sum_{i=1}^{6}\{(\nabla\times\boldsymbol{\omega})K_j + \mathbf{L}_j\}. \end{aligned} \tag{10}$$

Here the upper limit 6 in the summation denotes the number of faces of the volumetric cell element taken. Let us consider the surface integral term over one planar panel since the corresponding integral terms for other panels can be evaluated in the same manner. We drop the subscript j in K_j and $\mathbf{L}_j$ for simplicity of notation. The integral K represents induced potentials due to dipole distributions of the second order in density and source distributions with linearly varying density over the bounding surfaces. The integral has been evaluated in various manners by numerous researchers. Bai and Yeung [22] have set up the basic framework for treating the potential and the normal potential induced by a source density distribution which varies linearly over a triangular patch element (see also [23–25]). Herein on the basis of Bai and Yeung's procedure, we take the approach described in literature [25] for consistency with the present work. The analysis schemes are based on transformation of the associated integrals.

Let us take, for example, $\phi = 0{\cdot}5x^2$ as a simple choice of ϕ in Equation (9). In order to specify the second order variation of dipole density μ and the linear variation of source density σ over the respective planar panels of the bounding surfaces, we take a local coordinate system (ξ, η, ζ) such that the integration surface is in the plane $\zeta = 0$ and the direction of the ζ-axis is the same as that of the normal vector $\mathbf{n}$. The other two axes are on the surface and their directional unit vectors $(\mathbf{e}_\xi, \mathbf{e}_\eta)$ with the normal vector $(\mathbf{n})$ form a right-handed triple of orthogonal unit vectors. We can specify the dipole distribution as $\mu = 0{\cdot}5\{x_0 + \xi(\mathbf{e}_\xi \cdot \mathbf{i})\}^2$ and the source distribution as $\sigma = \{x_0 + \xi(\mathbf{e}_\xi \cdot \mathbf{i})\}(\mathbf{n}\cdot\mathbf{i})$, where x_0 is the x-coordinate of the origin of the local coordinate system and $\mathbf{e}_\xi = \mathbf{n}\times(\mathbf{i}\times\mathbf{n})/|\mathbf{i}\times\mathbf{n}|$. The integrands involved in

Equation (9) can now be transformed into either the curl form of a vector or the cross product of a vector with the normal **n**, as follows [26, 27]

$$\mathbf{n}\cdot\nabla\left(\frac{1}{r}\right) = -\mathbf{n}\cdot(\nabla\times\mathbf{A}), \tag{11}$$

$$(\xi - x_r)\mathbf{n}\cdot\nabla\left(\frac{1}{r}\right) = -z_r\left\{\mathbf{e}_\eta\cdot\mathbf{n}\times\nabla\left(\frac{1}{r}\right)\right\}, \tag{12}$$

$$(\xi - x_r)^2\mathbf{n}\cdot\nabla\left(\frac{1}{r}\right) = z_r\left\{\frac{1}{r} - \mathbf{e}_\xi\cdot\nabla\left(\frac{\xi - x_r}{r}\right)\right\}, \tag{13}$$

$$\frac{1}{r} = \mathbf{e}_n\cdot(\nabla\times\mathbf{B}), \tag{14}$$

$$\frac{\xi - x_r}{r} = \mathbf{e}_\eta\cdot(\mathbf{n}\times\nabla r), \tag{15}$$

with

$$\mathbf{A} = \frac{\mathbf{e}_n\times\mathbf{r}}{r(r + \mathbf{e}_n\cdot\mathbf{r})}, \qquad \mathbf{B} = \frac{\mathbf{e}_n\times\mathbf{r}}{(r + \mathbf{e}_n\cdot\mathbf{r})},$$

where the coordinates (x_r, y_r, z_r) of the field point are measured with respect to the origin of this local coordinate system, and $\mathbf{e}_n$ is a constant unit vector, which is independent of the integration variables of the surface integral. Note that Equations (12), (13) and (15) have been derived under the hypothesis of planarity of the surfaces. While Equations (11) and (14) hold for any $\mathbf{e}_n$ independent of the integration variables, the unit vector $\mathbf{e}_n$ is conveniently taken as $\pm\mathbf{n}$ in order to use Stokes's theorem where the sign is chosen such that the term $\mathbf{e}_n\cdot\mathbf{r}$ in the numerator of **A** and **B** is non-negative.

The integral K can then be written as, with the constants $a_0 = x_0 + x_r(\mathbf{e}_\xi\cdot\mathbf{i})$ and $a_1 = \mathbf{e}_\xi\cdot\mathbf{i}$ for shortness of expressions,

$$K = (\mathbf{n}\cdot\mathbf{i})(a_0\phi_\sigma^{(0)} + a_1\phi_\sigma^{(1)}) + 0{\cdot}5a_0^2\phi_\mu^{(0)} + a_0a_1\phi_\mu^{(1)} + 0{\cdot}5a_1^2\phi_\mu^{(2)},$$

where

$$\phi_\sigma^{(0)} = -\sum_{i=1}^{4} b_i K^{(1)}, \qquad \phi_\sigma^{(1)} = -\sum_{i=1}^{4} s_{i\eta} K^{(2)},$$

$$\phi_\mu^{(0)} = -\sum_{i=1}^{4} b_i(\mathbf{n}\cdot\mathbf{e}_n)\frac{E - K^{(1)}}{e}, \qquad \phi_\mu^{(1)} = -z_r\sum_{i=1}^{4} s_{i\eta}E,$$

$$\phi_\mu^{(2)} = -z_r\left[\phi_\sigma^{(0)} + \sum_{i=1}^{4}\{\mathbf{e}_\xi\cdot(\mathbf{s}_i\times\mathbf{n})K^{(3)}\}\right],$$

and the upper limit 4 in the summation denotes the number of sides of the panel. Similar to the two-dimensional cases, we can treat the associated line integrals for the sides of the quadrilateral planat surface independently by using the geometric parameters of each side.

Taking the local coordinate system (x', y'), as shown in Figure 2 for the evaluation of the line integrals, we may obtain the following closed-form expressions of the associated integrals by using the integral formulae [21, pp. 81–84]:

$$K^{(1)} = \int_0^{\ell_i} \frac{1}{\sqrt{(x'-\xi)^2 + y'^2} + e}\,\mathrm{d}\xi = E - \frac{e}{\sqrt{y'^2 - e^2}}\beta,$$

$$K^{(2)} = \int_0^{\ell_i} \sqrt{(x'-\xi)^2 + y'^2}\,\mathrm{d}\xi = \tfrac{1}{2}\{(\ell_i - x')r_{i+1} + x' r_i + y'^2 E\},$$

$$K^{(3)} = (\xi_i - x_r)E + s_{i\xi}(r_{i+1} - r_i + x' E),$$

$$E = \log \frac{r_{i+1} + \ell_i - x'}{r_i - x'},$$

$$\beta = \begin{cases} \arcsin H & \text{if } F > 0, \\ \pi - \arcsin H & \text{if } F \leqslant 0, \end{cases}$$

$$H = \frac{\sqrt{y'^2 - e^2}\{y'^2 \ell_i + e(\ell_i - x')r_i + e x' r_{i+1}\}}{y'^2 (r_i + e)(r_{i+1} + e)},$$

$$F = \left(\frac{y'^2 + e r_i}{r_i + e}\right)^2 + \left(\frac{y'^2 + e r_{i+1}}{r_{i+1} + e}\right)^2 - y'^2,$$

$$b_i = (\mathbf{n} \times \mathbf{r}) \cdot \mathbf{s}_i, \qquad s_{i\xi} = \mathbf{s}_i \cdot \mathbf{e}_\xi, \qquad s_{i\eta} = \mathbf{s}_i \cdot \mathbf{e}_\eta, \qquad e = \mathbf{e}_n \cdot \mathbf{r}.$$

Recall that $\mathbf{s}_i$ denotes the unit directional vector along the path of integration. In certain cases, some evaluations require special treatment. While the term $K^{(2)}$ is bounded, the term $K^{(1)}$ might be indeterminate if the field point lies on the same plane as the panel or on one of the lines defining the panel edge. In this respect, let us investigate the behavior of the term $b_i K^{(1)}$ in the vicinity of the panel sides. If $|y'|$ is equal to e, we have

$$K^{(1)} = E - \frac{x'}{r_i + e} - \frac{\ell_i - x'}{r_{i+1} + e}$$

but the factor b_i vanishes and, hence, the term $b_i K^{(1)}$ also vanishes. Furthermore, when y' is very small (accordingly the factor e approaches zero), b_i and $b_i K^{(1)}$ vanish in the same limit. When the field point approaches one of the vertices (*i.e.*, as $x' \to 0$ and $y' \to 0$) $K^{(1)}$ is logarithmically infinite, but $b_i K^{(1)}$ vanishes. Thus the integral K has a finite value even if the field point is on the same plane as the panel.

Next we will evaluate the second integral term $\mathbf{L}$ in Equation (10)

$$\mathbf{L} = -\int_S \mathbf{n} \times \left(\frac{1}{r}\,\boldsymbol{\omega}\right) \mathrm{d}S = \int_S \frac{\gamma \mathbf{t}}{r}\,\mathrm{d}S, \tag{16}$$

where $\gamma \mathbf{t} = -\mathbf{n} \times \boldsymbol{\omega}$.

Similar to the integral K, Equation (16) has the same form as the expression for the induced potential due to a source distribution over a surface. For the cases of distributions of vorticity with linearly varying densities within an element domain, γ has a linear variation over the surface being an integration region. With a specified linear distribution $\gamma\mathbf{t} = c_0\mathbf{t}_0 + c_1(\xi - x_r)\mathbf{t}_1 + c_2(\eta - y_r)\mathbf{t}_2$, we have

$$\mathbf{L} = c_0\mathbf{t}_0 \int_S \frac{1}{r}\,\mathrm{d}S + c_1\mathbf{t}_1 \int_S \frac{\xi - x_r}{r}\,\mathrm{d}S + c_2\mathbf{t}_2 \int_S \frac{\eta - y_r}{r}\,\mathrm{d}S. \tag{17}$$

Herein the vectors $\mathbf{t}_0$, $\mathbf{t}_1$ and $\mathbf{t}_2$ are brought outside the integral, because they are the constant vectors which are uniquely determined from the linearly varying distribution of vorticity density over the panel. The integrands in Equation (17) can now be transformed, as given in Equations (14) and (15), and

$$\frac{\eta - y_r}{r} = -\mathbf{e}_\xi \cdot (\mathbf{n} \times \nabla r).$$

Consequently Equation (17) can be written as

$$\mathbf{L} = \sum_{i=1}^{4} \{c_0\mathbf{t}_0 b_i K^{(1)} + (c_1\mathbf{t}_1 s_{i\eta} - c_2\mathbf{t}_2 s_{i\xi})K^{(2)}\}.$$

For constant distributions of vorticity, we only need to include the term $\mathbf{L}$ without the term K.

4. Examples

4.1. Two-dimensional lid-driven cavity flows

As an application of the present scheme, we consider a vorticity-based integro-differential formulation for the numerical solution of a two-dimensional cavity flow driven by shear and body forces (see Figure 3) [28, 29]. The shear motion of the lid of the cavity and the body force are prescribed as, respectively,

$$\begin{aligned} f(x) &= x^4 - 2x^3 + x^2 \\ \mathbf{f}_b &= 8\mu[24F(x) + 2f'(x)g''(y) + f'''g(y)]\mathbf{j} \\ &\quad +64[F_2(x)G_1(y) - g(y)g'(y)F_1(x)]\mathbf{j}, \end{aligned}$$

where

$$g(y) = y^4 - y^2, \qquad F(x) = \int_0^x f(x)\,\mathrm{d}x, \qquad F_1(x) = f(x)f''(x) - [f'(x)]^2,$$
$$F_2(x) = 0{\cdot}5f^2(x), \qquad G_1(y) = g(y)g'''(y) - g'(y)g''(y).$$

This lid-driven square cavity flow is a standard benchmark for testing numerical schemes in the context of computational fluid dynamics because of its simplicity and the availability of the analytical solution. The governing equations for the unsteady flow of an incompressible Newtonian fluid can be written as,

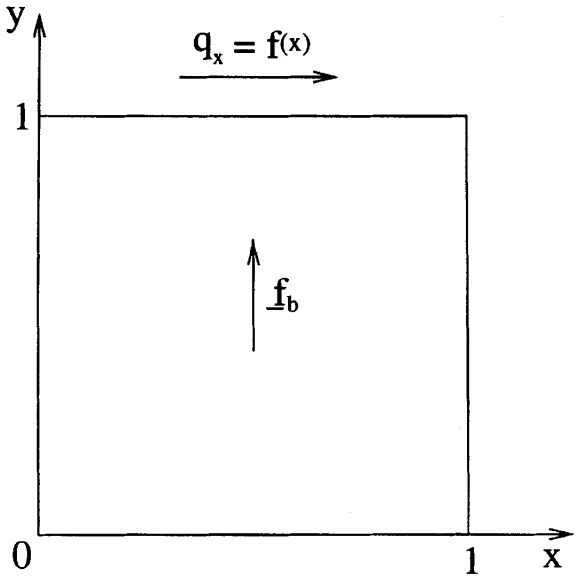

Figure 3. Coordinates and geometry for driven cavity.

$$\nabla \cdot \mathbf{q} = 0,$$

$$\boldsymbol{\omega} = \nabla \times \mathbf{q},$$

$$\frac{\partial \boldsymbol{\omega}}{\partial t} + \mathbf{q} \cdot \nabla \boldsymbol{\omega} = \boldsymbol{\omega} \cdot \nabla \mathbf{q} + \nu \nabla^2 \boldsymbol{\omega} + \nabla \times \mathbf{f}_b,$$

$$\nabla^2 \left(\frac{p}{p} + \tfrac{1}{2} q^2 \right) = \nabla \cdot (\mathbf{q} \times \boldsymbol{\omega} + \mathbf{f}_b),$$

The corresponding integro-differential vorticity-velocity formulation is given, in non-dimensional form, by,

$$\frac{\partial \omega}{\partial t} + \nabla \cdot (\mathbf{q}\omega) = \frac{1}{\mathrm{Re}} \nabla^2 \omega, \tag{18}$$

$$\mathbf{q} = \mathbf{q}_o - \frac{1}{2\pi} \int_S \boldsymbol{\omega} \times \nabla (\log r)\, \mathrm{d}S, \tag{19}$$

$$\begin{aligned} H \;=\; & -\frac{1}{2\pi} \int_C \left[H \frac{\partial (\log r)}{\partial n} - \frac{\partial H}{\partial n} \log r \right] \mathrm{d}C \\ & + \frac{1}{2\pi} \int_S \nabla \cdot (\mathbf{q} \times \boldsymbol{\omega} + \mathbf{f}_b) \log r \; \mathrm{d}S, \end{aligned} \tag{20}$$

where p is the pressure, ν the kinematic viscosity, ρ the density of the fluid, Re the Reynolds number and ω the scalar plane component of the vorticity vector ($\boldsymbol{\omega} \equiv \omega \mathbf{k}$). The velocity

term $\mathbf{q}_o$ in Equation (19) represents the contribution from the velocity distributions over the boundary (C) of the cavity, namely

$$\mathbf{q}_o = \int_C [(\mathbf{n}\cdot\mathbf{q})\nabla G + (\mathbf{n}\times\mathbf{q})\times\nabla G]\,\mathrm{d}C,$$

where $\mathbf{n}$ is the unit normal pointing into the fluid at the boundary C. The pressure p is related to the total pressure defined by

$$H = \frac{p - p_r}{\rho} + \tfrac{1}{2}(q^2 - q_r^2),$$

where the constants p_r and q_r are the reference pressure and velocity, respectively. In such a formulation, we deal with the Biot–Savart integral in order to compute the velocity from a vorticity distribution in the square cavity and to solve the total pressure in a boundary integral approach.

The boundary conditions for the velocity, the vorticity and the pressure supplement the system of Equations (18), (19) and (20). The no-slip velocity condition states that the velocity of the fluid $(\mathbf{q})$ is equal to the moving velocity $(\mathbf{U}_B)$ of the boundary $(\mathrm{f}x_B)$ of the cavity

$$\mathbf{q}(\mathbf{x}_B, t) = \mathbf{U}_B \quad \text{on } C.$$

We may derive the boundary condition for the vorticity flux (σ) at the boundary by taking the cross product of the Navier–Stokes equations with $\mathbf{n}$ and by using the velocity adherence condition:

$$\sigma \equiv -\frac{1}{\mathrm{Re}}\frac{\partial\omega}{\partial n} = -\mathbf{k}\cdot\mathbf{n}\times\left(\frac{\mathrm{d}\mathbf{U}_B}{\mathrm{d}t} + \nabla p - \mathbf{f}_b\right) \quad \text{on } C. \tag{21}$$

Similarly, the scalar product of the Navier–Stokes equations with $\mathbf{n}$ gives an expression for $\partial H/\partial n$ as

$$\frac{\partial H}{\partial n} = -\mathbf{n}\cdot\left(\frac{\partial\mathbf{q}}{\partial t} - \mathbf{q}\times\boldsymbol{\omega} + \frac{1}{\mathrm{Re}}\nabla\times\boldsymbol{\omega} - \mathbf{f}_b\right) \quad \text{on } C. \tag{22}$$

The computational procedures for the solution of the above system of the governing equations can be summarized in the following algorithm. (For details, see [30].)

(i) Integrate the vorticity transport equation (18) in time with enforcement of the no-slip condition. At the nth time step (corresponding to time t) the velocity and the vorticity fields are assumed to be computed (respecting the no-slip condition), we then seek to advance the solution to the $(n+1)$ time step (time $t + \Delta t$). A finite volume discretization is applied to Equation (18) which results in a consistent approximation to the conservation law, where the time rate of change of the vorticity within a domain is balanced by the net fluxes of the convective and the diffusive terms across the boundary surface of the domain. The entire physical fluid domain is divided into a finite number of small elements, each element serving as a computational cell. The discretized solution to Equation (18) results in a set of cell-averaged vorticity variables which is in balance with the face-averaged fluxes across the cell sides. The no-slip boundary condition is enforced in this stage by assigning the vorticity flux at the solid surface. The vorticity flux at the surface is assigned as its time-averaged value during a small time interval. An iterative process is required to introduce a proper amount of the

time-averaged vorticity flux in order to ensure the no-slip condition and to accordingly update ω^{n+1}. The spurious slip velocity is computed by performing the Biot–Savart integration for the vorticity field obtained at the present iterative stage.

(ii) Evaluate the Biot–Savart integral by using the integration scheme proposed in Section 2 in order to obtain the velocity field $\mathbf{q}^{n+1}$ which corresponds to the currently updated vorticity field ω^{n+1}. The vorticity is assumed to be distributed with a uniform strength over an individual cell element. Since the process of the Biot–Savart integration is repeated for all time steps, it is desirable to save computing time by storing the results of the Biot–Savart integral for a unit vorticity-distribution over an individual cell.

(iii) Solve the integral equation for H^{n+1} by using the values for $\mathbf{q}^{n+1}$ and ω^{n+1} obtained in steps (i) and (ii). Substituting Equation (22) for $\partial H/\partial n$ in Equation (20) as a field point approaches the boundary points of the cavity yields a Fredholm integral equation of the second kind for H

$$\tfrac{1}{2}H + \frac{1}{2\pi}\int_C H\frac{\partial(\log r)}{\partial n}\,\mathrm{d}C = \frac{1}{2\pi}\int_C \frac{1}{\mathrm{Re}}\frac{\partial \omega_B}{\partial s}\log r\,\mathrm{d}C - \frac{1}{2\pi}\int_S (\mathbf{q}\times\boldsymbol{\omega}+\mathbf{f}_b)\cdot\boldsymbol{\nabla}(\log r)\,\mathrm{d}S, \tag{23}$$

where the integrals over C are evaluated in the sense of the Cauchy principal value integral and $\partial\omega_B/\partial s$ is the gradient of the boundary vorticity (ω_B) in the direction (s) tangent to the boundary

One possible approach for solving Equation (23) numerically for the total pressure is to use a panel-method approximation. We use herein a straight-line element for the body contour subdivision representation, and a uniform density distribution of singularity strength on each panel at the boundary and over each cell in the fluid domain. The surface integral term on the right-hand side of Equation (23) is similar in form to the Biot–Savart integral in Equation (19) if we replace $(\mathbf{q}\times\boldsymbol{\omega})\cdot\boldsymbol{\nabla}(\log r)$ with $\boldsymbol{\omega}\times\boldsymbol{\nabla}(\log r)$. In order to include the influence of the field distribution of $(\mathbf{q}\times\boldsymbol{\omega})$, the algorithm for evaluation of the Biot–Savart integral described in Section 2 can be used under the assumption that the distribution is piecewisely constant over each cell element. Consequently Equation (23) deduces a set of algebraic expressions with unknown values for the total pressure on the panels.

Since the vorticity flux is related to the tangential gradient of the pressure along the body surface and the normal gradient of the total pressure is incorporated with the tangential gradient of the body vorticity at the current time, we employ the iterative calculation between the vorticity flux and the pressure on the boundary until they reach a converged state. Up to this point, we can invoke the principle of conservation of vorticity by integrating Equation (21). The result must be zero, since the pressure is inherently a single-valued function, which leads to the argument that the total vorticity in the fluid domain is always zero.

(iv) Advance the calculation to the next time step by repeating steps (i), (ii) and (iii).

The above solution procedure is summarized in Figure 4. For purposes of comparison with the exact steady-state solution, the calculations are advanced to steady-state. As the initial condition in the time evolution of the flow, an impulsive start was formulated. A uniform grid of equal size that divides the cavity flow region was used. The vorticity, the vorticity flux, and the pressure distributions along the cavity wall for $\mathrm{Re} = 100$ with variation of the time interval and the grids are shown in Figures 5 and 6, where the agreement with the exact solution is excellent. Figure 7 shows that the time evolution of the velocity along the vertical and the

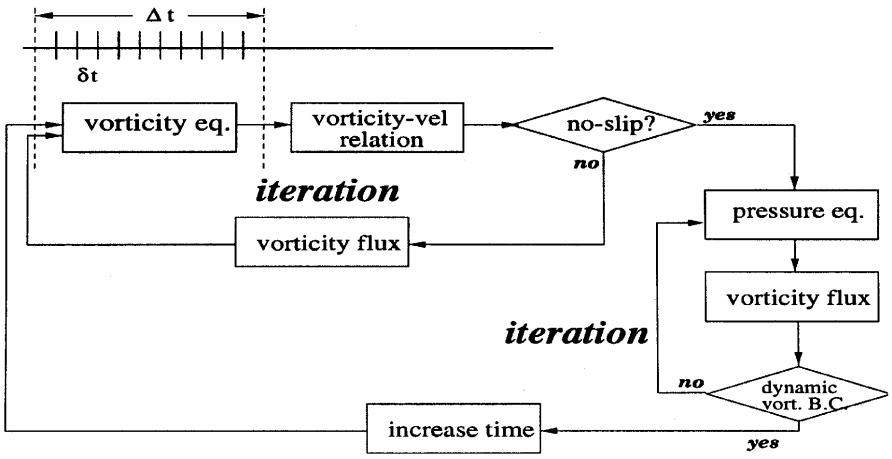

Figure 4. Flow chart for solution procedure in the present vorticity-velocity formulation

horizontal center lines of the cavity at Re $= 100$ with $\Delta t = 0{\cdot}05$ and the 61×61 grid. Figure 8 shows the time evolution of kinetic energy for cavity flow in this case. This is compared with the exact steady-state value $1216/33075(= 0{\cdot}0367650)$. The streamline pattern, the vorticity contour, and the pressure contour in the steady-state are shown in Figure 9, where the agreement is again very good (It is difficult to distinguish between the exact solution and the numerical solution with the present scheme). The above comparison implies that the evaluation of the Biot–Savart integral works well. In the present numerical implementation, for a vorticity distribution with unit density over each cell element, we compute the induced velocities at desired field points once (namely, at centroids of neighboring cell elements) and then save them (within the limit of computer memory capacity) so that the time-consuming calculations at successive time steps can be avoided.

4.2. TOKAMAK COILS

Consider a typical tokamak field coil (with peripheral current of 24 A) of rectangular cross section $0{\cdot}45\,\text{m} \times 0{\cdot}5\,\text{m}$, as shown in Figure 10 the half of the coil in the symmetric plane, consisting of three circular arc segments whose radii are indicated in Figure 10. This current distribution corresponds to the vorticity distribution $\omega\mathbf{e}_\theta$ and its linear variation then becomes $\nabla \times \omega\mathbf{e}_\theta = \omega/\rho\mathbf{k}$, where $\omega = 24$ and $\mathbf{e}_\theta$ is the unit base vector in the circumferential direction in a cylindrical coordinate system (ρ, θ, z). The field coil has been subdivided into finite straight segments (volumetric elements) of $2 * (N_1 + N_2 + N_3) \times M$ where N_1, N_2 and N_3 are the number of the elements (with uniformly angular openings) subdivided in the θ-direction for the first (I), the second (II) and the third (III) circular arc segment in Figure 10, respectively, and M is the number of the elements subdivided in the ρ-direction. There is no subdivision in the z-direction. Figure 11 shows the magnetic field q_z on a perimeter $0{\cdot}1\,\text{m}$ inside the field coil, computed with the closed-form expressions presented in Section 3. This is given by a sum over the partial fields generated by each element. To validate the formulas derived in the present paper, we have taken two cases of piecewise constant distributions (Case 1) and piecewise linear distributions (Case 2) for the subdivided elements. We conclude that, as the number of the subdivided elements increases, the accuracy improves and the field values for both cases tend to have converged values.

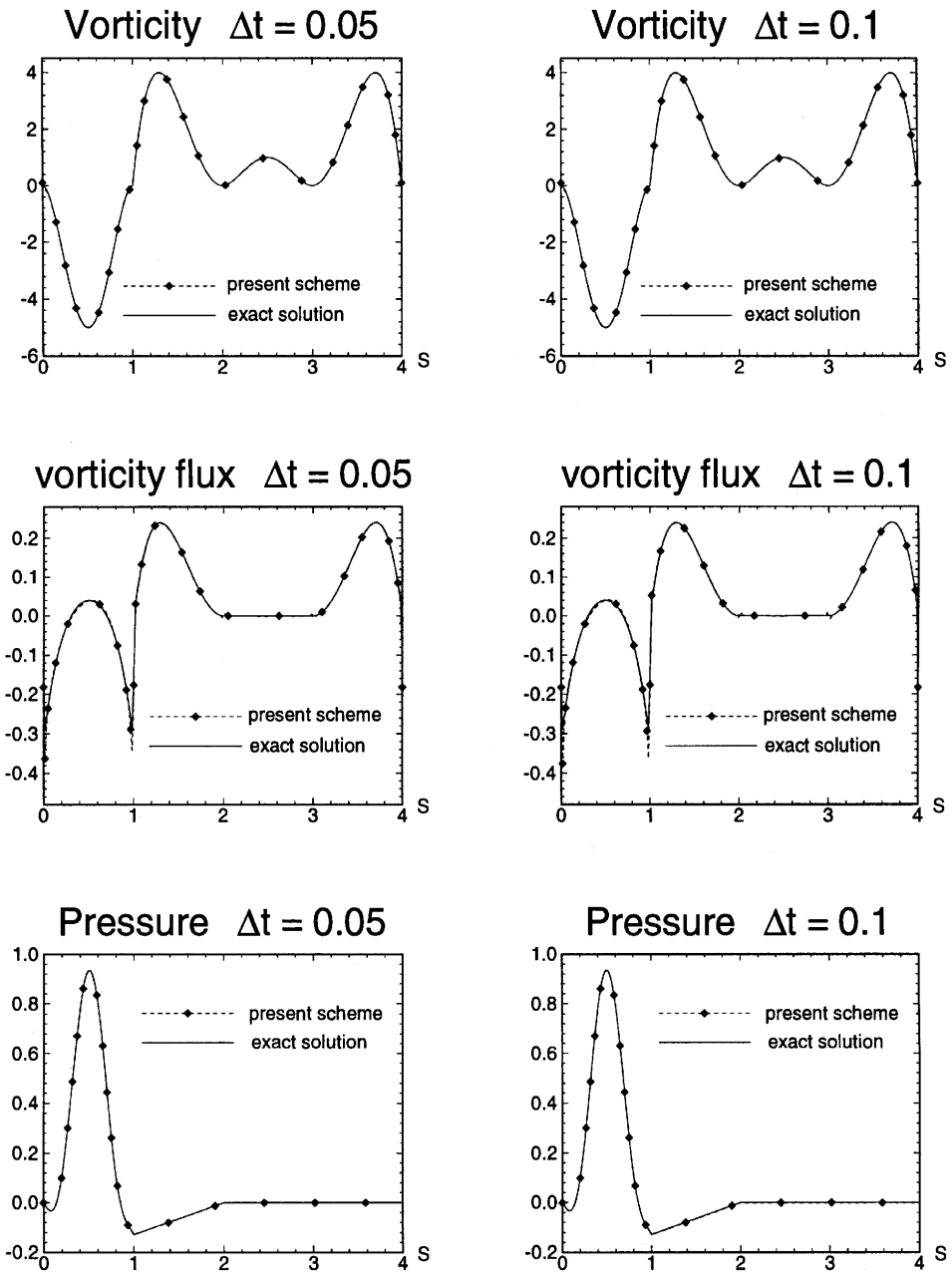

Figure 5. Sensitivity of time interval on vorticity, vorticity flux and pressure along the cavity wall for Re = 100 with the 61 × 61 grid. The perimeter(S) along the cavity wall has the clockwise direction from the origin at the upper left corner of the cavity.

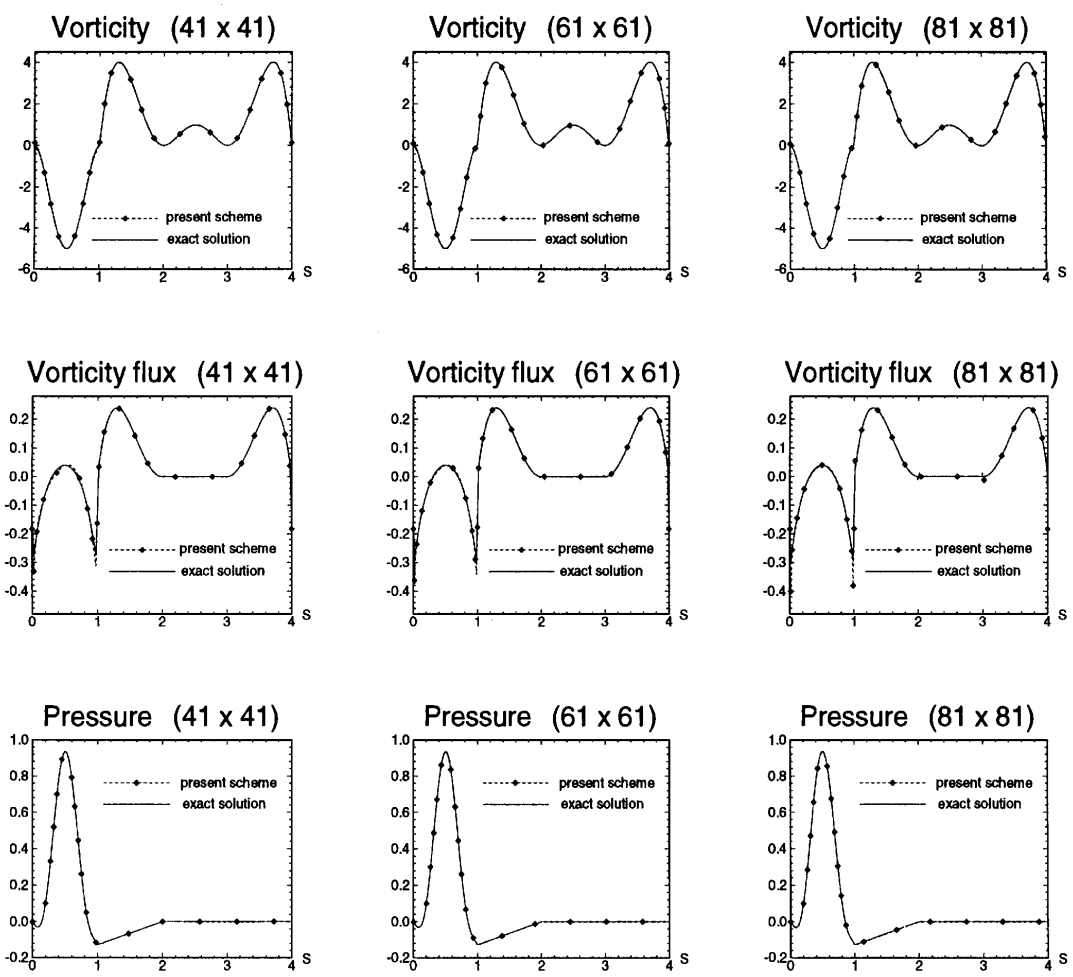

Figure 6. Sensitivity of mesh size on vorticity, vorticity flux and pressure along the cavity wall for Re = 100 with $\Delta t = 0{\cdot}05$.

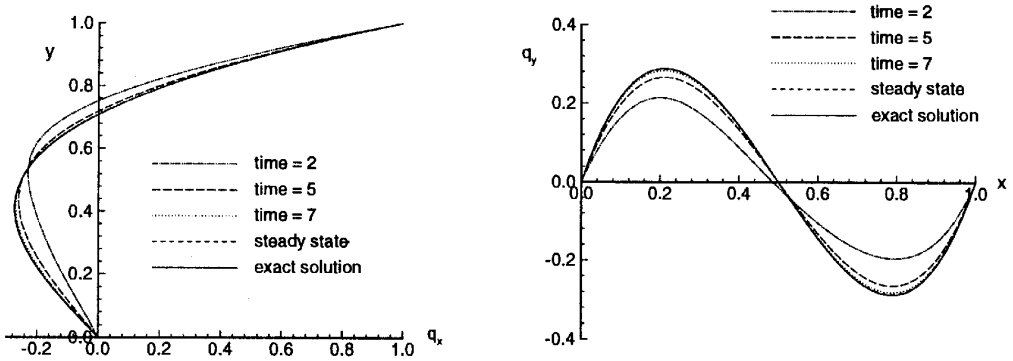

Figure 7. Time evolution of the velocity along the center lines of the cavity for Re = 100 with $\Delta t = 0{\cdot}05$ and the 61×61 grid.

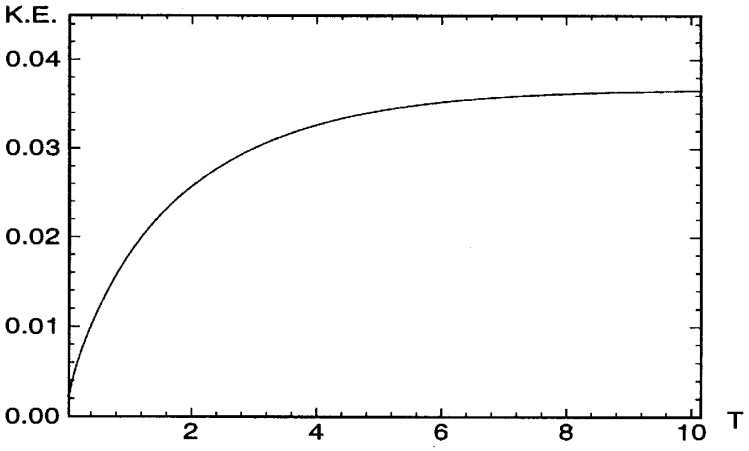

Figure 8. Time evolution of kinetic energy for Re = 100 with $\Delta t = -0{\cdot}05$, and the 61×61 grid.

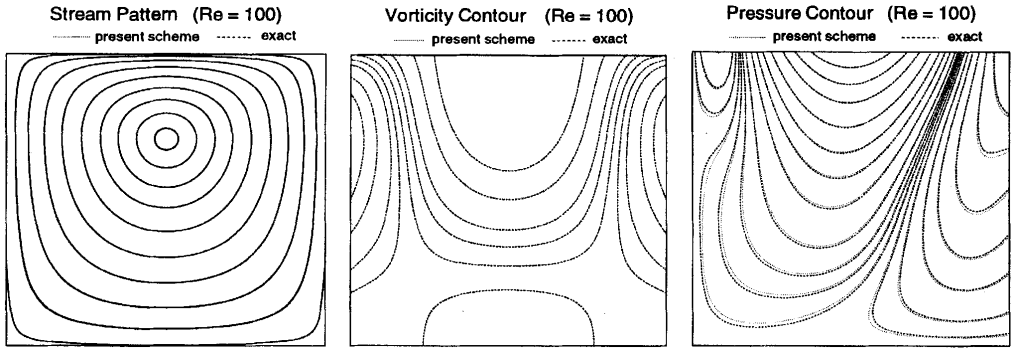

Figure 9. Streamline pattern, vorticity contour and pressure contour for Re = 100 with $\Delta t = 0{\cdot}05$ and the 61×61 grid.

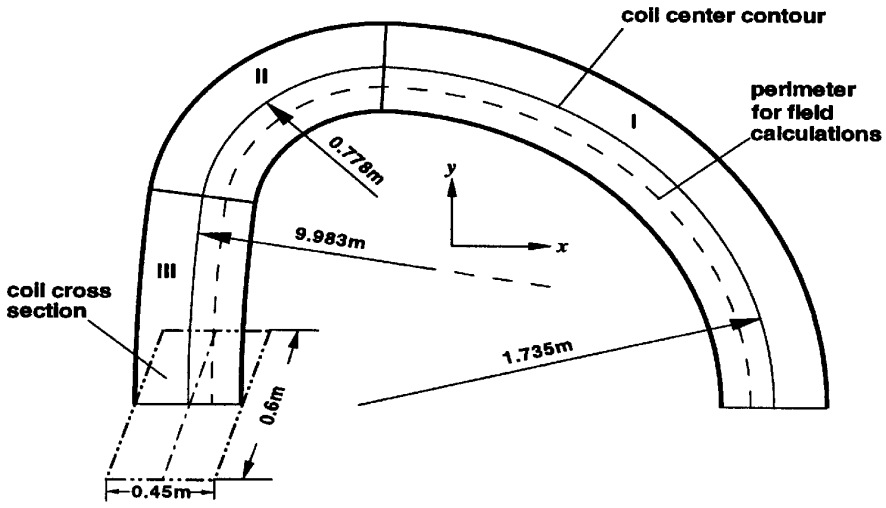

Figure 10. View for the half of a typical tokamak coil in the symmetric plane.

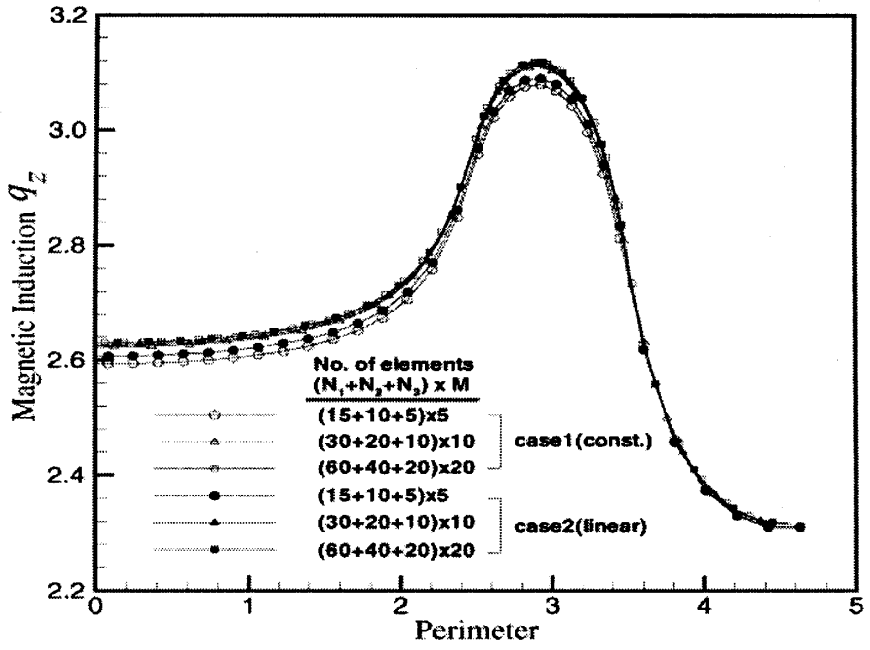

Figure 11. Magnetic field (q_z) on a perimeter inside the field coil of rectangular cross section in the symmetry plane for a typical tokamak coil.

5. Higher-order variations

5.1. TWO-DIMENSIONS

The previous sections deal with the case where the density of vorticity is constant and/or linear. We will show a systematic extension of the present analysis to higher-order polynomial variations. Let us first consider the general integral form for the higher-order variations of vorticity density in two-dimensions

$$I_{m,n} = \int_S \frac{(\xi - x)^m (\eta - y)^n}{r^2} \, \mathrm{d}S.$$

The powers m and n of the coordinates (ξ, η) of an integration point are arbitary non-negative integers. $I_{1,0}$, $I_{0,1}$, $I_{2,0}$, $I_{1,1}$ and $I_{0,2}$ can be evaluated from the preceding results in Section 2. By appropriately transforming the integrands for $I_{m,n}$ into appropriate ones and by applying the Gauss theorem for the transformed surface integral, we can deduce the relation

$$\begin{aligned} I_{m,n} \;=\; & \mathbf{j} \cdot \oint_C \mathbf{s} \log r (\xi - x)^{m-1} (\eta - y)^n \, \mathrm{d}C \\ & + \frac{m-1}{n+1} \mathbf{i} \cdot \oint_C \mathbf{s} \log r (\xi - x)^{m-2} (\eta - y)^{n+1} \, \mathrm{d}C \\ & + \frac{m-1}{n+1} I_{m-2,n+2}. \end{aligned}$$

To be complete, $I_{m,0}$, $I_{m,1}$, $I_{0,n}$ and $I_{1,n}$ must be eventually evaluated. After transforming the involved integrands, *e.g.*, of $I_{m,0}$ and $I_{m,1}$, into the form,

$$\begin{aligned}\frac{(\xi - x)^m}{r^2} &= \mathbf{j}\cdot\mathbf{k}\times\nabla\left\{(\xi - x)^{m-1}\left(\log r + \frac{1}{m}\right)\right\} \\ &\quad -\frac{m-1}{m}\nabla\cdot\{(\xi - x)^{m-2}\mathbf{r}\log r\}, \\ \frac{(\xi - x)^m(\eta - y)}{r^2} &= -\mathbf{i}\cdot\mathbf{k}\times\nabla\{(\xi - x)^m\log r\},\end{aligned}$$

we have the results

$$\begin{aligned}I_{m,0} &= \frac{1}{m}\mathbf{j}\cdot\oint_C \mathbf{s}(\log r + 1)(\xi - x)^{m-1}\,\mathrm{d}C \\ &\quad +\frac{m-1}{m}\mathbf{i}\cdot\oint_C \mathbf{s}(\xi - x)^{m-2}(\eta - y)\log r\,\mathrm{d}C, \\ I_{m,1} &= -\mathbf{i}\cdot\oint_C \mathbf{s}(\xi - x)^m\log r\,\mathrm{d}C,\end{aligned}$$

$$\begin{aligned}I_{0,n} &= -\frac{1}{n}\mathbf{i}\cdot\oint_C \mathbf{s}(\log r + 1)(\eta - y)^{n-1}\,\mathrm{d}C \\ &\quad -\frac{n-1}{n}\mathbf{j}\cdot\oint_C \mathbf{s}(\xi - x)(\eta - y)^{n-2}\log r\,\mathrm{d}C, \\ I_{1,n} &= \mathbf{j}\cdot\oint_C \mathbf{s}(\eta - y)^n\log r\,\mathrm{d}C.\end{aligned}$$

5.2. THREE-DIMENSIONS

The corresponding extension of the three-dimensional Biot–Savart integral is possible in a manner similar to the two-dimensional case. Let us take a general form of the higher-order distributions with arbitrary non-negative powers m, n, p of the coordinates (ξ, η, ζ) of an integration point,

$$I_{m,n,p} = \int_V \frac{(\xi - x)^m(\eta - y)^n(\zeta - z)^p}{r^3}\,\mathrm{d}V.$$

We can then obtain the recursive relation

$$\begin{aligned}I_{m,n,p} &= -\mathbf{j}\cdot\mathbf{k}\times\oint_S \mathbf{n}\frac{(\xi - x)^{m-1}(\eta - y)^n(\zeta - z)^p}{r}\,\mathrm{d}S \\ &\quad -\frac{m-1}{n+1}\mathbf{i}\cdot\mathbf{k}\times\oint_S \mathbf{n}\frac{(\xi - x)^{m-2}(\eta - y)^{n+1}(\zeta - z)^p}{r}\,\mathrm{d}S \\ &\quad +\frac{m-1}{n+1}I_{m-2,n+2,p}. \qquad (24)\end{aligned}$$

As in the two-dimensional case, we decrease values of (m, n, p) recursively until the desired integrals are obtained. The integrals with $m + n + p \leqslant 2$ can be evaluated from the results in Section 3. It is only necessary to calculate, namely, the integral $I_{m,1,p}$, $I_{m,0,0}$

$$I_{m,1,p} = \mathbf{i} \cdot \mathbf{k} \times \oint_S \mathbf{n} \frac{(\xi - x)^m (\zeta - z)^p}{r} \, \mathrm{d}S,$$

$$I_{m,0,0} = \mathbf{i} \cdot \mathbf{k} \times \oint_S \mathbf{n} \left[\mathbf{i} \cdot \mathbf{k} \times \nabla \left\{ \frac{(\xi - x)^m r}{(\xi - x)^2 + (\zeta - z)^2} \right\} \right] \mathrm{d}S.$$

Other necessary integrals such as $I_{1,n,p}$, $I_{0,n,0}$, $I_{m,n,1}$ can be evaluated in the same manner as that in which the integration variables are replaced by one other in cyclic order. The surface integrals in Equation (24) (which represent the velocity potentials induced by higher-order distributions of source singularities over a surface) can be reduced to contour integrals as has been shown by Newman [24], if the bounding surface is composed of (approximated by) planar surfaces. In fact, closed-form expressions for the evaluation of the resulting (contour) integrals might be complicated but straightforward. A detailed evaluation is not considered in the present work.

6. Concluding remarks

The Biot–Savart integral which has been evaluated in the preceding sections is a fundamental part of vorticity formulations in computational fluid dynamics and of numerical codes for solving certain problems arising in the field of electromagnetic field theory. From the standpoint of practical implementation, the efficient evaluation of this integral is essential if the number of elements used to represent a computation domain is large. Simple expressions for the evaluation of the Biot–Savart integral have been derived, which are suitable for the computation of velocity field issued from a given vorticity distribution for vorticity-based numerical methods in hydro- and aerodynamics. The simplicity of these expressions results from the transformation of the integrands, subject to the restriction that vorticity distributions are those of constant and/or linear density over an element whose boundaries are planar surfaces (straight lines in two-dimensional). With the transformed integrands, Gauss's and Stokes's integral theorems can be used in order to reduce the multiple order of the involved integrals to a single order integral. The resulting expressions are given in closed-forms after the evaluation of the line integrals along the element boundary edges. The expressions show a distinct advantage in versatility over the method of numerical integration or existing analytical expressions. A computer algorithm for their evaluation can be constructed in a more unified manner. Although we have considered a volumetric element with six planar faces (a quadrilateral panel with four sides in two-dimensional), the analysis presented can be applied directly to elements with an arbitrary number of faces (sides) by using the same procedure. An integro-differential vorticity-velocity formulation in computational fluid dynamics was applied to two-dimensional lid-driven cavity flow problems, in which the two-dimensional Biot–Savart integral is essentially incorporated. A typical tokamak coil conductor was taken as a good example to validate the present expressions. A systematic extension of the present analysis can be performed for the cases of higher-order variations of vorticity density.

Acknowledgments

The present research is a combination of both previous and current works. The author wishes to acknowledge the financial support of the Korea Research Foundation made in the Program Year 1997–99 (Grant no. 97-02-00-01-01-3).

References

1. J. L. Hess and A. M. O. Smith, Calculation of non-lifting potential flow about arbitrary three-dimensional bodies. *J. Ship Res.* 8 (1964) 22–44.
2. J. L. Hess and A. M. O. Smith, Calculation of potential flow about arbitrary bodies. *Progr. Aeronaut. Sci. Series* 8 (1966) 1–138.
3. B. Bodner, H. Köfler and J. Sammer, 3-dimensional magnetic field calculation for an arrangement of s.c. coils with an outer magnetic core. *IEEE Trans. Magn.* 28 (1992) 1402–1405.
4. G. K. Batchelor, *An Introduction to Fluid Dynamics*. Cambridge: CUP (1967) 615pp.
5. P. G. Saffman, *Vortex Dynamics*. Cambridge: CUP (1992) 311pp.
6. P. M. Gresho, Incompressible fluid dynamics: some fundamental formulation issues. *Annu. Rev. Fluid Mech.* 23 (1991) 413–453.
7. L. M. Urankar, Vector potential and magnetic field of current-carrying finite arc segment in analytical form–Part I: Filament approximation. *IEEE Trans. Magn.* 16 (1980) 1283–1288.
8. J. E. Kerwin and C.-S. Lee, Prediction of steady and unsteady marine propeller performance by numerical lifting-surface theory. *SNAME Trans.* 86 (1978) 218–253.
9. L. M. Urankar, Vector potential and magnetic field of current-carrying finite arc segment in analytical form–Part II: Thin sheet approximation. *IEEE Trans. Magn.* 18 (1982) 911–917.
10. Z. M. Cielak and R. B. Kinney, Analysis of unsteady viscous flow past an airfoil–Part II: Numerical formulation and results. *AIAA J.* 16 (1978) 105–110.
11. J.-C. Suh, *Unsteady Analysis for a Two-dimensional Foil in Uniformly Sheared Onset Flow*. Ph.D. thesis., Univ. of Michigan (1990) 140pp.
12. I. N. Kirshner, *The Bilinear Triangular Vorticity Patch.* Univ. of Michigan, Informal notes (unpublished) (1989) 32pp.
13. R. D. Graglia, On the numerical integration of the linear shape functions times the 3-D Green's function or its gradient on a plane triangle. *IEEE Trans. Antennas Propagat.* 41 (1983) 1448–1455.
14. D. R. Wilton, S. M. Rao, A. W. Glisson, D. H. Schaubert, O. M. Al-Bundak and C. M. Butler, Potential integrals of uniform and linear source distributions on polygonal and polyhedral domains. *IEEE Trans. Antennas Propagat.* AP-32 (1984) 276–281.
15. L. M. Urankar, Vector potential and magnetic field of current-carrying finite arc segment in analytical form–Part III: Exact computation for rectangular cross section. *IEEE Trans. Magn.* 18 (1982) 1860–1867.
16. S. Babic and M. M. Gavrilovic, New expression for calculating magnetic fields due to current-carrying solid conductors. *IEEE Trans. Magn.* 33 (1997) 4134–4136.
17. C. F. Weggel and D. P. Schwartz, New analytic formulas for calculating magnetic fields. *IEEE Trans. Magn.* 24 (1988) 1544–1547.
18. L. Morino, Helmholtz and Poincaré potential-vorticity decompositions for the analysis of unsteady compressible viscous flows. In: P. K. Banerjee and L. Morino (eds), *Boundary Element Methods in Nonlinear Fluid Dynamics. Developments in Boundary Element Methods-6.* Elsevier Applied Science (1990) pp. 1–54.
19. I. R. Ciric, New models for current distributions and scalar potential formulations of magnetic filed problems. *J. Appl. Phys.* 61 (1987) 2709–2717.
20. I. R. Ciric, Simple analytic expressions for the magnetic field of current coils. *IEEE Trans. Magn.* 27 (1991) 669–673.
21. I. S. Gradshteyn and I. M. Ryzhik, *Table of Integrals, Series and Products.* New York and London: Academic Press Inc. (1965) 1086pp.
22. K. J. Bai and R. W. Yeung, Numerical solutions to free-surface flow problems. *Proc. 10th Symp. Naval Hydro.* (1974) 609–647.
23. W. C. Webster, The flow about arbitrary, three-dimensional smooth bodies. *J. Ship Res.* 19 (1975) 206–218.

24. J. N. Newman, Distributions of sources and normal dipoles over a quadrilateral panel. *J. Eng. Math.* 20 (1986) 113–126.
25. J.-C. Suh, J.-T. Lee and S.-B. Suh, A bilinear source and doublet distribution over a planar panel and its application to surface panel methods. *Proc. 19th Symp. Naval Hydro.* (1992) 837–847.
26. J. P. Guiraud, Potential of velocities generated by a localized vortex distribution. *Aerospace Res.* ESA-TT-560 (1978) 105–107.
27. J.-C. Suh, Analytical evaluation of the surface integral in the singularity methods. *Trans. Soc. Naval Arch. Korea* 29 (1992) 1–17.
28. T. M. Shih, C. H. Tan and B. C. Hwang, Effects of grid staggering on numerical schemes. *Int. J. Numer. Meth. Fluids.* 9 (1989) 193–212.
29. S. Rida, F. Mckenty, F. L. Meng and M. Reggio, A staggered control volume scheme for unstructured triangular grids. *Int. J. Numer. Meth. Fluids.* 25 (1997) 697–717.
30. J.-C. Suh and K.-S. Kim, A vorticity-velocity formulation for solving the two-dimensional Navier–Stokes equations. *Fluid Dyn. Res.* 25 (1999) 195–216.